Linear Instability Waves in Supersonic Turbulent Mixing Layers

Saad A. Ragab* and J. L. Wu†
Virginia Polytechnic Institute and State University, Blacksburg, Virginia

The structures of supersonic turbulent mixing layers are assumed to be spatially growing instability waves superimposed on mean flows, which are also spatially diverging. The objective of the work presented here is to determine these waves and to evaluate the effect of certain parameters such as mean velocity and temperature profiles on the stability characteristics (growth rate, most amplified frequency, etc.). Linear inviscid stability theory of nonparallel mean flow has been used. Three-dimensional waves in the form of axisymmetric or helical modes interacting with the axisymmetric basic state are considered. The basic state is determined by solving the axisymmetric turbulent boundary-layer equations for the configuration of unconfined coaxial mixing. A mixing length model is used for turbulence closure. Increasing the Mach number of the outer stream or increasing the temperature of the inner stream (gas generator) significantly reduces the growth rate and gain along the mixing layer length.

I. Introduction

THE scramjet engine cycle in which combustion of liquid fuels takes place at supersonic speeds has been recognized as an efficient propulsive cycle for missiles and airplanes cruising at hypersonic speeds.[1-3] Since the early experimentation in the 1950's that demonstrated the feasibility of combustion of liquid fuels in a supersonic airstream, efforts have resulted in a hybrid engine cycle called the Dual-Combustion Ramjet (DCR).[4] In this cycle, roughly 25% of the supersonic inlet flow is decelerated down to subsonic (or sonic) speed and directed into a "dump combustor" or gas generator. All of the fuel then is injected into the high-temperature subsonic stream resulting in a very fuel-rich mixture and, hence, ignition and combustion can be maintained. However, the combustion process of the unreacted fuel has to be completed in a supersonic combustor downstream of the gas generator after mixing with the supersonic airstream previously diverted by the inlet.

The propulsive efficiency of the DCR cycle will be affected by the quality of mixing taking place in the shear layer that is formed by the subsonic (or sonic) stream issuing from the gas generator and the supersonic stream surrounding it. As pointed out by Waltrup, "Our current understanding of the mechanisms governing and/or controlling the mixing and combustion processes when two sonic or supersonic streams merge to form a free shear layer...is very limited."[3] Thus, there is a need to investigate the structure, growth, and means of controlling supersonic turbulent mixing layers in nonreactive and reactive flows. The present work is a step toward the understanding of turbulent mixing layers.

In this section we briefly discuss previous theoretical efforts that use hydrodynamic stability theory as a means of investigating the structures of mixing layers and their response to external excitations.

Basic Features of Mixing Layers

It has been experimentally established that the spreading rates (and, hence, entrainment and mixing) of supersonic turbulent mixing layers are substantially lower than those of incompressible layers (e.g., Refs. 5 and 6). Moreover, the basic structures of incompressible layers are well defined. Linear instability waves prevail in the initial stage of development, followed by formation of large-scale coherent vortical motion and, finally, pairing or amalgamation of these vortices (e.g., Ref. 7). Thus, the mixing process is governed by the coherent structures that are predominantly spanwise vortices; however, spanwise waviness and small-scale streamwise vortices also have been experimentally observed.[8,9]

In supersonic mixing layers, the structure is much less understood. Ikawa and Kubota[5] investigated a single-stream supersonic mixing layer. From the measured energy spectra, they found that the coherent structures (spectral peaks) disappear with increasing Reynolds number and with boundary-layer trip roughness, which imply a fully developed layer at the trailing edge of the plate. They concluded that the structure of fully developed supersonic turbulent, free mixing layers consists of a randomly fluctuating field with no concentration of high-intensity large-scale wave motions in a preferred frequency range. Recently, however, Chinzei et al.[6] conducted experiments on two-stream supersonic layers and presented, among other results, spark schlieren photographs of flowfields that show the presence of large-scale vortical structures similar to but weaker and displaced somewhat farther downstream of the splitter plate than those observed by Brown and Roshko[10] for the low-speed case. The presence of large-scale structures in supersonic mixing layers also has been reported by the most recent experimental work on the subject by Papamoschou and Roshko.[11] This is a very significant result because it suggests the possibility of exciting the layer so that these structures might be enhanced and appear sooner than in the natural case. This point has been advocated by Ho and Huang,[12] who showed that the spreading of a mixing layer can be greatly manipulated by exciting the layer near a subharmonic of the most amplified frequency.

Instability Waves as a Model of Coherent Structures in Free Shear Layers

The approach adopted in this paper is motivated primarily by the successful attempts of Gaster et al.,[13] Wygnanski and Petersen,[14] and Wygnanski et al.,[15] among others, in capturing coherent motions in free shear layers as instability waves superimposed on turbulent mean velocity profiles. Gaster et al. applied linear inviscid stability theory to measured mean flow profiles of forced mixing layers. Excellent agreement between theory and experiment was obtained for the eigenfunctions, but the agreement for the growth rates was much less satisfactory. They attributed this discrepancy to nonlinear effects. Recently, Wygnanski and Petersen reported similar results for axisymmetric jets and small-deficit wakes. They also summarized the results of a nonlinear theory due to Cohen,[16] which

Presented as Paper 87-1418 at the AIAA 19th Fluid Dynamics, Plasmas Dynamics, and Lasers Conference, Honolulu, HI, June 8-10, 1987; received July 6, 1987; revision received April 11, 1988.

*Associate Professor, Department of Engineering Science and Mechanics. Member AIAA.
†Graduate Student, Department of Engineering Science and Mechanics. Member AIAA.

led to surprisingly accurate predictions for the spreading rate of the externally excited turbulent shear layer. These successful attempts indicate that the role played by small-scale structures in the overall development of free shear layers is not significant.

With a different objective in mind, Tam and Morris[17] and Tam and Burton[18] also applied inviscid linear stability theory to measured mean flow profiles of supersonic turbulent mixing layers. They were interested in the radiated sound due to the coherent motions in the layer. An excellent and comprehensive review of jet instability is given by Michalke.[19]

In this paper, we consider linear inviscid instability waves on a coaxial mixing layer. The inner stream (which we call the gas generator) has a nozzle radius r_0^*, while the outer stream (which we call the primary flow) is unconfined. The mean turbulent velocity and temperature profiles are computed by solving the boundary-layer equations. Computing the mean flow gives control over the range of parameters (temperature ratio, velocity ratio, Mach number, etc.) affecting the instability problem.

II. Mathematical Formulation

The governing equations of the basic state and instability waves are presented. Cylindrical polar coordinates (x,r,θ) are used. The equations are written in terms of dimensionless variables defined by $(r,x) = (r^*,x^*)/r_0^*$, $(u,v,w) = (u^*,v^*,w^*)/U_\infty^*$, $\rho = \rho^*/\rho_\infty^*$, $T = T^*/T_\infty^*$, $p = p^*/\rho_\infty^* U_\infty^{*2}$, $H = H^*/C_p^* T_\infty^*$, and $\mu = \mu^*/\mu_\infty^*$, where r_0^* is the nozzle radius, and U_∞^*, ρ_∞^*, T_∞^*, and μ_∞^* are the freestream $(r\to\infty)$ values of velocity, density, temperature, and viscosity, respectively. The Mach number is given by $M = U_\infty^*/a_\infty^*$, and the Reynolds number by $Re = \rho_\infty^* U_\infty^* r_0^*/\mu_\infty^*$, where a_∞^* is the speed of sound in the freestream.

Mean Flow Calculations

The mean turbulent velocity and temperature profiles in the coflowing mixing layer are obtained by solving the axisymmetric boundary-layer equations. Viscid-inviscid interaction between the outer inviscid flow and the shear layer is neglected, and the mean pressure is assumed to be uniform throughout the flowfield. Letting U and V denote the axial and radial velocity components, respectively, and R, $\bar{T}$, and H denote the density, temperature, and total enthalpy, we write the governing equations of the basic state in the form (e.g., Ref. 20)

$$\frac{\partial}{\partial x}(rRU) + \frac{\partial}{\partial r}(rRV) = 0 \tag{1}$$

$$rRU\frac{\partial U}{\partial x} + rRV\frac{\partial U}{\partial r} = \frac{1}{Re}\frac{\partial}{\partial r}\left[r(\mu+\mu_T)\frac{\partial U}{\partial r}\right] \tag{2}$$

$$rRU\frac{\partial H}{\partial x} + rRV\frac{\partial H}{\partial r} = \frac{1}{Re}\frac{\partial}{\partial r}\left\{r(\mu Pr^{-1} + \mu_T Pr_T^{-1})\frac{\partial H}{\partial r} + (\gamma-1)M^2[(1-Pr^{-1})\mu + (1-Pr_T^{-1})\mu_T]U\frac{\partial U}{\partial r}\right\} \tag{3}$$

$$\bar{T} = 1 \tag{4}$$

Equations (1–4) are the continuity, momentum, energy, and state equations, respectively. The laminar and turbulent Prandtl numbers are assigned the values $Pr = 0.72$ and $Pr_T = 0.75$. A linear viscosity-temperature relation is assumed for the laminar viscosity μ, hence

$$\mu = \bar{T} \tag{5}$$

The turbulent viscosity μ_T is determined from a mixing length formula used by Dash et al.[21] and Hasen[22]:

$$\mu_T = Re\, R\ell^2 \left|\frac{\partial U}{\partial r}\right| \tag{6}$$

where ℓ is the mixing length, which is related to the local value of the mixing-layer thickness δ by

$$\ell = 0.065\delta \tag{7}$$

The thickness δ is the distance between the radial locations where the vorticity $\partial U/\partial r$ is 10% of its maximum value across the layer. This definition also is used downstream of the potential core region. All of the mean flow results presented in this paper are obtained at $Re = 1000$.

The boundary conditions imposed on the mean flow are

$$\frac{\partial U}{\partial r} = 0, \quad \frac{\partial T}{\partial r} = 0, \quad V = 0 \quad \text{at } r = 0 \tag{8}$$

$$U = 1, \quad \bar{T} = 1 \quad \text{as } r\to\infty \tag{9}$$

Initial conditions at $x = 0$ are specified by the top-hat profiles

$$U = \begin{cases} U_G & r \le 1 \\ 1 & r > 1 \end{cases} \tag{10}$$

$$\bar{T} = \begin{cases} T_G & r \le 1 \\ 1 & r > 1 \end{cases} \tag{11}$$

A second-order implicit finite-difference method is used to advance the solution in the x direction.

Linear Inviscid Stability Analysis

The following assumptions are adopted in deriving the disturbance equations:

1) The interaction between the instability wave and the small-scale turbulence is neglected, i.e., the small-scale turbulence enters the problem through the mean turbulent velocity and temperature profiles only.

2) The modification on the mean flow due to the passage of the wave, which is a nonlinear effect, also is neglected.

3) The disturbances satisfy the linearized equations of inviscid gas dynamics for a perfect gas.

4) The basic state is axisymmetric, and the nonparallelism is accounted for by the method of multiple scales.[23-28]

Let Q denote a mean flow quantity, and q denote a disturbance quantity; the total flow variables (basic state plus disturbances) are written as

$$\tilde{u} = U + u, \quad \tilde{v} = \epsilon V + v, \quad \tilde{w} = w$$

$$\tilde{\rho} = R + \rho, \quad \tilde{p} = (1/\gamma M^2) + p, \quad \tilde{T} = (1/R) + T \tag{12}$$

where T is the temperature disturbance. The mean flow quantities are functions of r and of a slow axial coordinate $x_1 = \epsilon x$ where ϵ is a small parameter characterizing the spreading rate of the shear layer or the radial velocity component; for example, $\epsilon = d\delta_m/dx$ where δ_m is the momentum thickness. Substituting the total flow, Eqs. (12), into the inviscid gas dynamics equations, dropping the nonlinear terms in the disturbances, and substracting the mean flow equations, we obtain

$$\frac{\partial \rho}{\partial t} + U\frac{\partial \rho}{\partial x} + R\left(\frac{\partial u}{\partial x} + \frac{\partial v}{\partial r} + \frac{1}{r}\frac{\partial w}{\partial \theta} + \frac{v}{r}\right) + v\frac{\partial R}{\partial r} + \rho\frac{\partial U}{\partial x} + u\frac{\partial R}{\partial x} + \frac{1}{r}\frac{\partial}{\partial r}(\rho r \epsilon V) = 0 \tag{13}$$

$$\frac{\partial u}{\partial t} + U\frac{\partial u}{\partial x} + v\frac{\partial U}{\partial r} + \frac{1}{R}\frac{\partial p}{\partial x} + u\frac{\partial U}{\partial x} + \epsilon V\frac{\partial u}{\partial r} + \frac{\rho}{R}\left(U\frac{\partial U}{\partial x} + \epsilon V\frac{\partial U}{\partial r}\right) = 0 \tag{14}$$

$$\frac{\partial v}{\partial t} + U\frac{\partial v}{\partial x} + \frac{1}{R}\frac{\partial p}{\partial r} + \epsilon V\frac{\partial v}{\partial r} + v\frac{\partial \epsilon V}{\partial r} + u\frac{\partial \epsilon V}{\partial x} + \frac{\rho}{R}\left(U\frac{\partial \epsilon V}{\partial x} + \epsilon V\frac{\partial \epsilon V}{\partial r}\right) = 0 \tag{15}$$

$$\frac{\partial w}{\partial t} + U\frac{\partial w}{\partial x} + \frac{1}{R}\frac{1}{r}\frac{\partial p}{\partial \theta} + \epsilon V\left(\frac{w}{r} + \frac{\partial w}{\partial r}\right) = 0 \tag{16}$$

$$R\left(\frac{\partial T}{\partial t} + U\frac{\partial T}{\partial x} + v\frac{\partial R^{-1}}{\partial r}\right) - (\gamma-1)M^2\left(\frac{\partial p}{\partial t} + U\frac{\partial p}{\partial x} + \epsilon V\frac{\partial p}{\partial r}\right) + \rho\left(U\frac{\partial R^{-1}}{\partial x} + \epsilon V\frac{\partial R^{-1}}{\partial r}\right) + R\left(u\frac{\partial R^{-1}}{\partial x} + \epsilon V\frac{\partial T}{\partial r}\right) = 0 \tag{17}$$

$$\gamma M^2 p = \frac{\rho}{R} + RT \tag{18}$$

Next we consider spatial stability and assume a propagating wave form for each disturbance quantity, e.g.,

$$q = [q_0(x_1,r) + \epsilon q_1(x_1,r) + \cdots]\exp(i\phi) \tag{19}$$

where ϕ is given by

$$\phi = \int \alpha(x_1)\frac{dx_1}{\epsilon} + m\theta - \omega t \tag{20}$$

where m is an integer, ω a real frequency, and α a complex wave number.

Substituting Eq. (19) into Eqs. (13–18) and equating the coefficients of like powers of ϵ, we obtain for $0(\epsilon^0)$

$$L_1(\rho_0,u_0,v_0,w_0) = -i\Omega\rho_0 + i\alpha R u_0 + R\frac{\partial v_0}{\partial r} + \frac{R}{r}v_0 + \frac{i\,m}{r}Rw_0 + \frac{\partial R}{\partial r}v_0 = 0 \tag{21a}$$

$$L_2(u_0,v_0,p_0) = -i\Omega u_0 + v_0\frac{\partial U}{\partial r} + \frac{i\alpha}{R}p_0 = 0 \tag{21b}$$

$$L_3(v_0,p_0) = -i\Omega v_0 + \frac{1}{R}\frac{\partial p_0}{\partial r} = 0 \tag{21c}$$

$$L_4(w_0,p_0) = -i\Omega w_0 + \frac{i\,m}{r}\frac{1}{R}p_0 = 0 \tag{21d}$$

$$L_5(v_0,p_0,T_0) = -i\Omega RT_0 + R\frac{\partial R^{-1}}{\partial r}v_0 + (\gamma-1)M^2 i\Omega p_0 = 0 \tag{21e}$$

$$L_6(\rho_0,p_0,T_0) = \gamma M^2 p_0 - \rho_0 R^{-1} - RT_0 = 0 \tag{21f}$$

and for $0(\epsilon^1)$, we obtain six equations of the form

$$L_n(q_1) = -B_n, \qquad n = 1,\ldots,6 \tag{22}$$

where

$$B_1 = U\frac{\partial \rho_0}{\partial x_1} + R\frac{\partial u_0}{\partial x_1} + \rho_0\frac{\partial U}{\partial x_1} + u_0\frac{\partial R}{\partial x_1} + \frac{1}{r}\frac{\partial}{\partial r}(\rho_0 rV) \tag{23a}$$

$$B_2 = U\frac{\partial u_0}{\partial x_1} + \frac{1}{R}\frac{\partial p_0}{\partial x_1} + u_0\frac{\partial U}{\partial x_1} + V\frac{\partial u_0}{\partial r} + \frac{\rho_0}{R}\left(U\frac{\partial U}{\partial x_1} + V\frac{\partial U}{\partial r}\right) \tag{23b}$$

$$B_3 = U\frac{\partial v_0}{\partial x_1} + V\frac{\partial v_0}{\partial r} + v_0\frac{\partial V}{\partial r} \tag{23c}$$

$$B_4 = U\frac{\partial w_0}{\partial x_1} + V\left(\frac{w_0}{r} + \frac{\partial w_0}{\partial r}\right) \tag{23d}$$

$$B_5 = RU\frac{\partial T_0}{\partial x_1} - (\gamma-1)M^2\left(U\frac{\partial p_0}{\partial x_1} + V\frac{\partial p_0}{\partial r}\right) + \rho_0\left(U\frac{\partial R^{-1}}{\partial x_1} + V\frac{\partial R^{-1}}{\partial r}\right) + R\frac{\partial R^{-1}}{\partial x_1}u_0 + RV\frac{\partial T_0}{\partial r} \tag{23e}$$

$$B_6 = 0 \tag{23f}$$

where $\Omega = \omega - \alpha U$.

Solution to the $0(\epsilon^0)$ Problem

Since x_1 appears in Eqs. (21a–21f) as a parameter, the solution to these equations can be written as

$$(p_0,v_0,u_0,w_0,\rho_0,T_0) = A(x_1)\zeta_n(x_1,r), \quad n = 1,6 \tag{24}$$

By using Eqs. (21b–21f), the variables (ζ_n, $n = 2,\ldots,6$) can be expressed in terms of ζ_1 and $\partial\zeta_1/\partial r$. Then Eq. (21a) can be written in terms of ζ_1 (or p_0) as

$$L(p_0) = p_0'' + \left(\frac{1}{r} - \frac{\Lambda'}{\Lambda}\right)p_0' - \left(\frac{m^2}{r^2} + \alpha^2 - M^2\Lambda\right)p_0 = 0 \tag{25}$$

where $\Lambda = \Omega^2 R$, and a prime denotes $\partial/\partial r$. The boundary conditions on p_0 are

$$p_0 \text{ is regular at } r = 0 \tag{26a}$$

$$p_0 \text{ is bounded as } r \to \infty \tag{26b}$$

In this paper the calculations are limited to spatially amplified disturbances $\alpha_i < 0$ and, hence, the critical point defined by $\Lambda = 0$ is off the real axis of the extended complex r plane. Near $r = 0$, $\Lambda' \to 0$ and $\Lambda \to \Lambda_0$, and the solution to Eq. (25) that satisfies Eq. (26a) is given by the modified Bessel function of the first kind $I_m(\hat{\alpha}_0 r)$, where $\hat{\alpha}_0 = (\alpha^2 - M^2\Lambda_0)^{1/2}$ with Real $(\hat{\alpha}_0) > 0$.

As $r \to \infty$, $\Lambda' \to 0$ and $\Lambda \to \Lambda_\infty$, and the solution to Eq. (25) that satisfies Eq. (26b) is given by the modified Bessel function of the second kind $K_m(\hat{\alpha}_\infty r)$, where $\hat{\alpha}_\infty = (\alpha^2 - M^2\Lambda_\infty)^{1/2}$ with Real $(\hat{\alpha}_\infty) > 0$.

The eigenvalue problem, Eqs. (25–26), is solved by a shooting technique. For given ω and mean flow conditions, a value of α is guessed. Equation (25) is then integrated in two sweeps by using a Runge-Kutta scheme. The first sweep starts near $r = 0$ (typically $r = 0.01$) and marches to $r = 1$. The second sweep starts at $r = r_{\max}$ (typically $r_{\max} = 3$) and marches to $r = 1$. In both sweeps, initial values for p_0 and p_0' are obtained from the appropriate modified Bessel functions. At $r = 1$, the continuity of p_0 and p_0' demands that

$$I_m = p_{01}p_{02}' - p_{01}'p_{02} = 0 \tag{27}$$

where subscripts 1 and 2 indicate the sweep numbers. A Newton-Raphson procedure is used to improve the guessed value of α by iterating on Eq. (27).

Solution to the $0(\epsilon^1)$ Problem

Following a procedure similar to that leading to Eq. (25), we write the equation for p_1 in the form

$$L(p_1) = F(x_1,r) \tag{28}$$

with boundary conditions

$$p_1 \text{ is regular at } r = 0 \tag{29a}$$

$$p_1 \text{ is bounded as } r \to \infty \tag{29b}$$

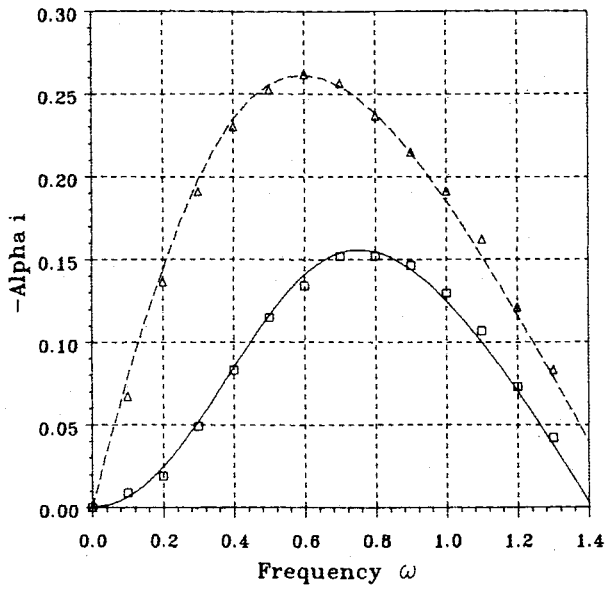

Fig. 1 Spatial growth rate $-\alpha_i$ vs ω. Michalke jet profile, $M = 1.2$, $T_G = 1$; —— $m = 0$, --- $m = 1$; symbols are Michalke's computation.[19]

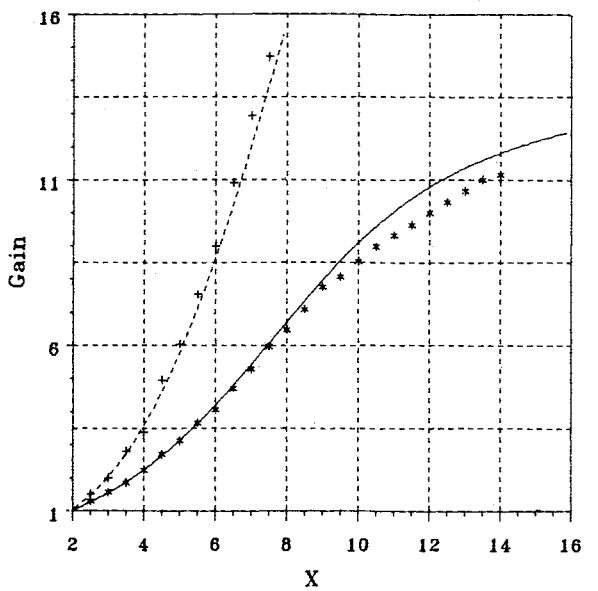

Fig. 2 Gain in the streamwise velocity component on $r = 0$. Michalke jet profile, $M = 0$, $T_G = 1$; —— $\omega = 0.6$, --- $\omega = 0.9$. Symbols are Crighton and Gaster results.[27]

The functional F is given by

$$F = H_1 \frac{dA}{dx_1} + H_2 A \tag{30}$$

where H_1 and H_2 are functionals of the mean flow and the solution to the $0(\epsilon^0)$ problem. The expression for H_1 can be simplified to

$$H_1 = -2i(\alpha + M^2 UR\Omega)\zeta_1 + 2i\omega U'\zeta_1'/\Omega^2 \tag{31}$$

Since the homogeneous problem $L(p_1) = 0$ with boundary conditions (29a) and (29b) has a nontrivial solution, the nonhomogeneous problem given by Eqs. (28) and (29a–29b) has a solution if the functional F satisfies a solvability condition (see, for example, Ref. 24), which is given by

$$\int_0^\infty \frac{r}{\Lambda} p_0 F \, dr = 0 \tag{32}$$

Substituting Eq. (30) into Eq. (32) and using $p_0 = A(x_1)\zeta_1$, we obtain

$$h_1 \frac{dA}{dx_1} + h_2 A = 0 \tag{33}$$

where

$$h_1 = \int_0^\infty \frac{r}{\Lambda} \zeta_1 H_1 \, dr \tag{34}$$

$$h_2 = \int_0^\infty \frac{r}{\Lambda} \zeta_1 H_2 \, dr \tag{35}$$

We write the solution to Eq. (33)

$$A = A_0 \exp\left(-\int_{x_0}^{x} \frac{\epsilon h_2}{h_1} dx\right) \tag{36}$$

where A_0 is the value of A at some initial position x_0.

To first order the pressure disturbance can be written as

$$p = A_0 \zeta_1(x,r) \exp\left[\int_{x_0}^{x} \left(i\alpha - \frac{\epsilon h_2}{h_1}\right) dx + i(m\theta - \omega t)\right] \tag{37}$$

and similar expressions can be written for u and v. A numerical value for ϵ can be absorbed in h_2 by replacing $\epsilon(\partial/\partial x_1)$ by $\partial/\partial x$ and ϵV by V.

It is well known[25,26] that the growth rate and wave number in nonparallel flows are not uniquely defined. The growth rate depends on the streamwise coordinate x and the transverse coordinate r; moreover, different physical quantities (pressure, velocity, density, etc.), may have different growth rates. Here we define a complex wave number $\bar{\alpha}$ for the disturbance q_n by

$$i\bar{\alpha}(x,r,\zeta_n) = \frac{1}{q_n}\frac{\partial q_n}{\partial x} \tag{38}$$

Using Eq. (37) we write Eq. (38) as

$$i\bar{\alpha}(x,r,\zeta_n) = i\alpha - \frac{\epsilon h_2}{h_1} + \frac{1}{\zeta_n}\frac{\partial \zeta_n}{\partial x} \tag{39}$$

We note that the first term on the right of Eq. (39), $i\alpha$, is the contribution from the quasiparallel theory; α is a function of x only. The term $\epsilon h_2/h_1$ also depends on x only, but the last term $\zeta_n^{-1}\,\partial\zeta_n/\partial x$ depends on x,r and the disturbance quantity being measured. It follows from Eq. (39) that the growth rate of the pressure is $-\alpha_i(x,r,\zeta_1)$, and the phase speed is $c_{ph} = \omega/\bar{\alpha}_r(x,r,\zeta_1)$. Similarly, for the streamwise velocity disturbance the growth rate is $-\bar{\alpha}_i(x,r,\zeta_3)$.

Finally, we define the gain of the disturbance quantity q_n by

$$\text{Gain}(x,r,q_n) = \exp\left[\int_{x_0}^{x} -\alpha_i(x,r,\zeta_n)\, dx\right] \tag{40}$$

Michalke Velocity Profile

Michalke[19] has proposed the mean velocity profile

$$U(x,r) = \tfrac{1}{2}U_0[1 + \tanh b(1/r - r)] \tag{41}$$

to describe the mean axial velocity of a jet with velocity U_0 at the nozzle exit and $b = r_0^*/4\delta_m^*$, where δ_m^* is a momentum thickness. According to Michalke, this form gives reasonable agreement with the profile measured by Crow and Champagne[29] around the station $x = 4$, provided b takes the value 25/16. Crighton and Gaster[27] generalized Eq. (41) for a slowly diverging jet by letting $\delta_m^* = (3x^* + 4r_0^*)/100$.

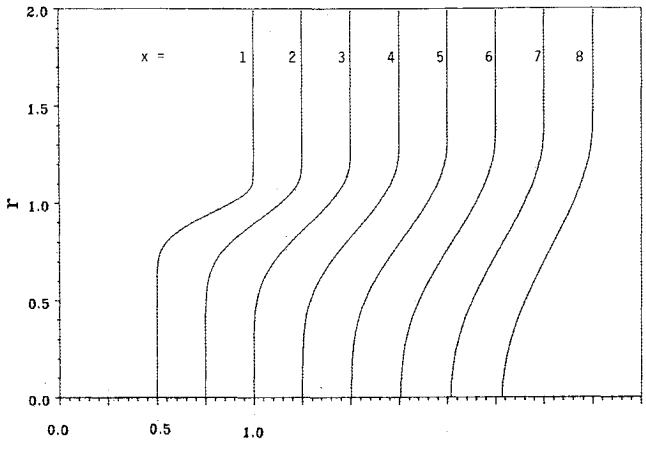

a) Streamwise velocity

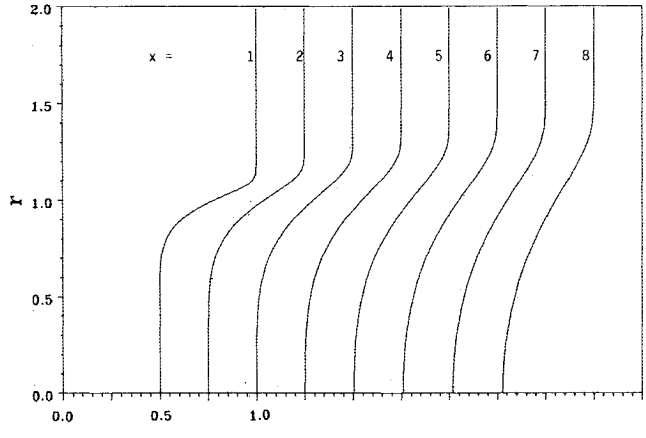

b) Density

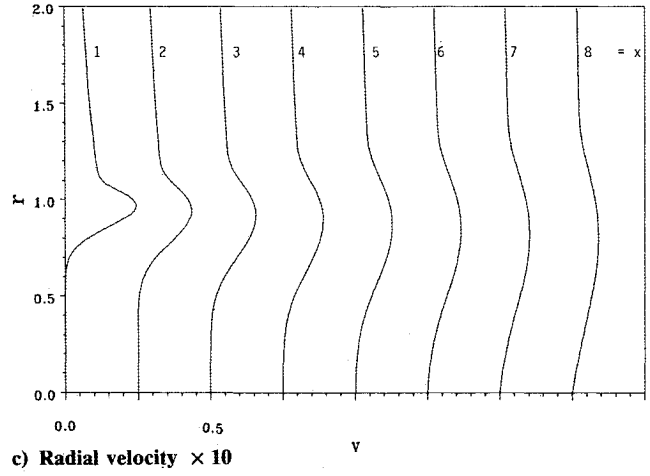

c) Radial velocity × 10

Fig. 3 Computed mean flow profiles in a coaxial mixing layer; $M = 2$, $U_G = 0.5$, $T_G = 2.0$ ($R_G = 0.5$).

III. Results

Comparison with Michalke Parallel Flow Calculations

The variation of the growth rate and phase speed with frequency has been computed for the jet profile given by Eq. (41) at a Mach number of 1.2 and compressible momentum thickness of $r_0^*/\delta_m^* = 5.97$, and the jet is assumed to be cold. The growth rates for the axisymmetric mode ($m = 0$) and the first azimuthal mode ($m = 1$) are compared with Michalke's results in Fig. 1. Our results are in full agreement with Michalke's results.[19]

Comparison with Crighton-Gaster Nonparallel Stability Calculations

Crighton and Gaster[27] computed the incompressible nonparallel spatial stability for the generalized Michalke profile.

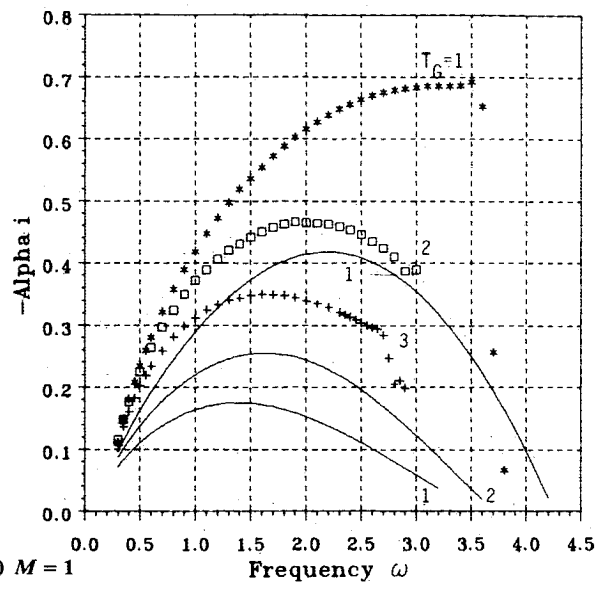

a) $M = 1$

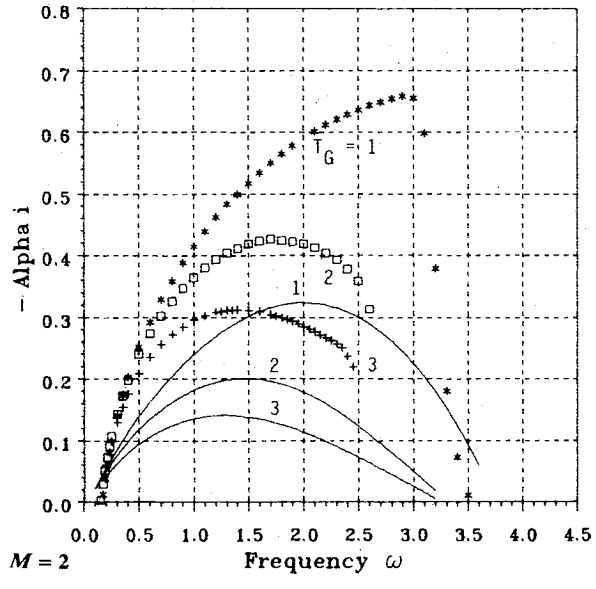

b) $M = 2$

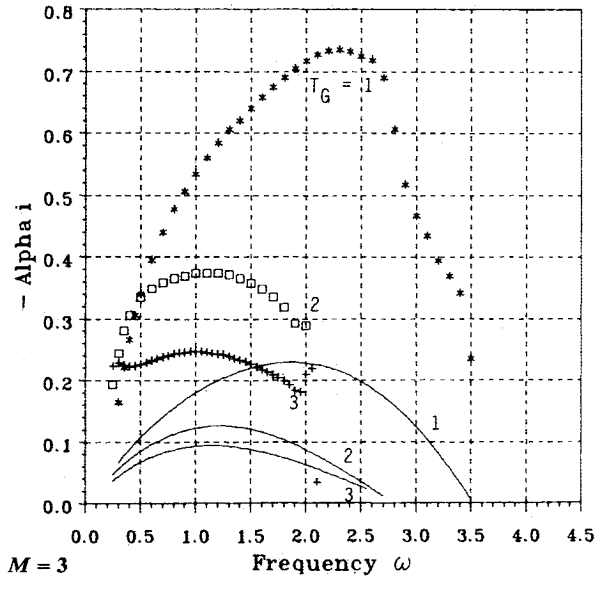

c) $M = 3$

Fig. 4 Axisymmetric mode $m = 0$. Growth rate $-\alpha_i$ vs frequency ω at $x = 2$. Symbols are predictions of nonparallel theory for pressure disturbance at $r = 0.9$.

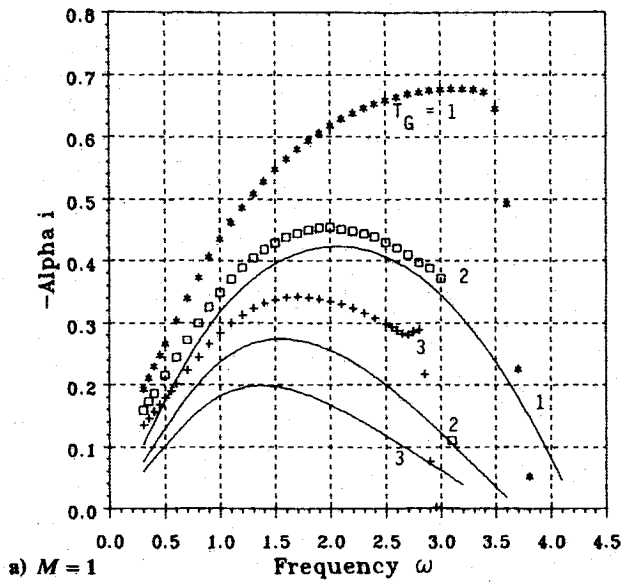

a) $M = 1$

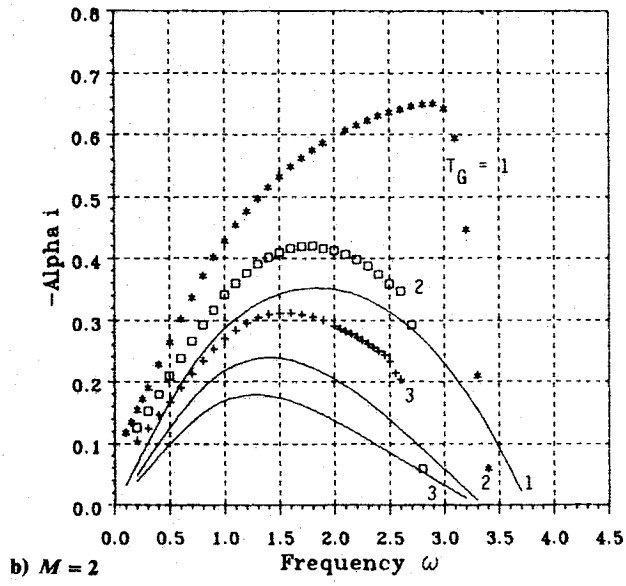

b) $M = 2$

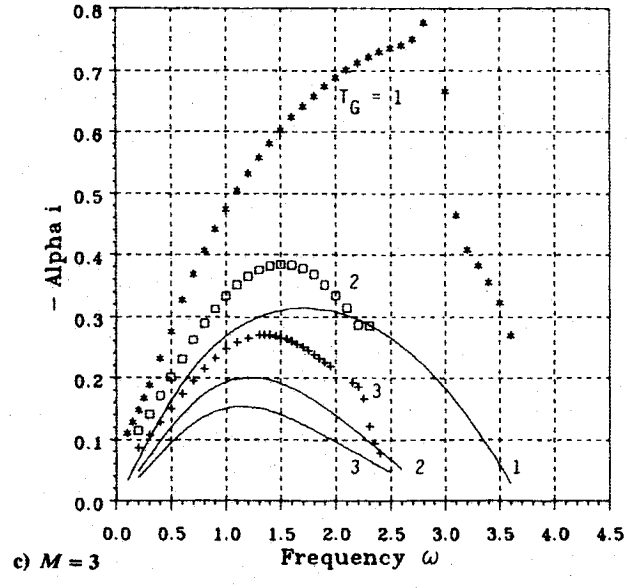

c) $M = 3$

Fig. 5 First azimuthal mode $m = 1$. Growth rate $-\alpha_i$ vs frequency ω at $x = 2$. Symbols are predictions of nonparallel theory for the pressure disturbance at $r = 0.9$.

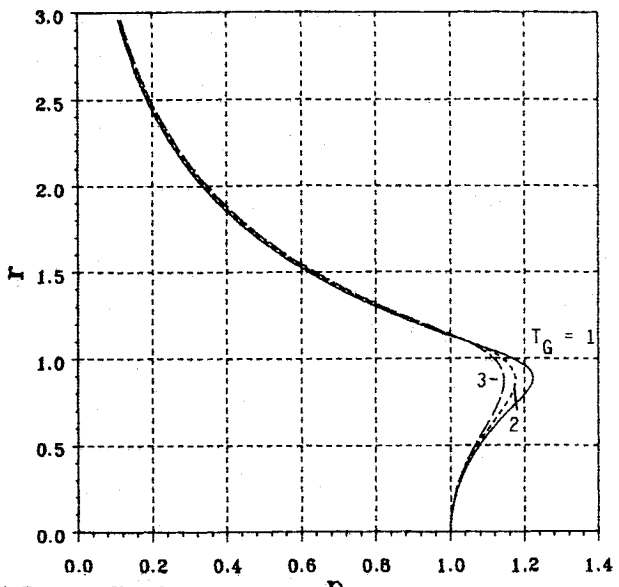

a) Pressure disturbance ζ_1

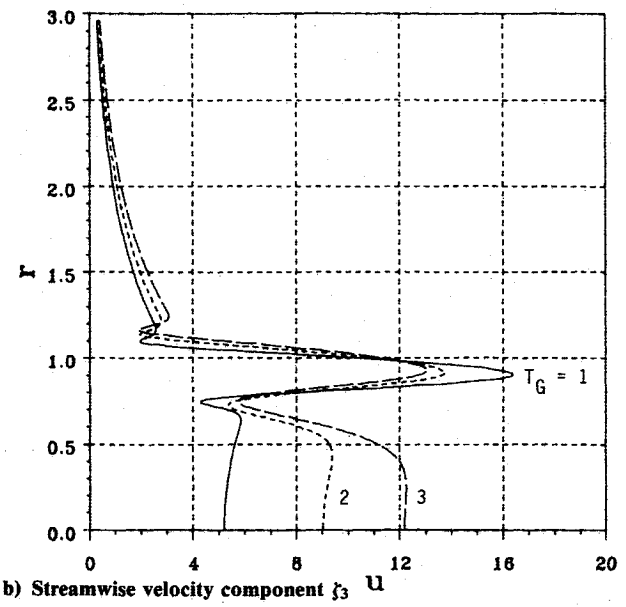

b) Streamwise velocity component ζ_3

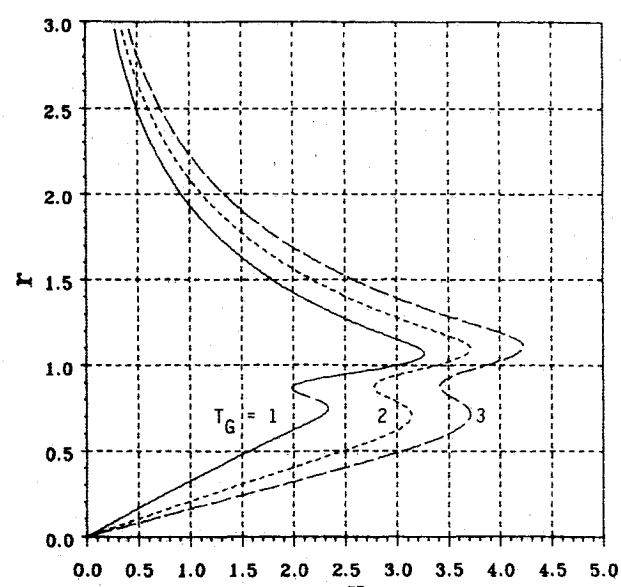

c) Transverse velocity component ζ_2

Fig. 6 Axisymmetric mode $m = 0$. Eigenfunctions at $x = 2$, $\omega = 0.8$.

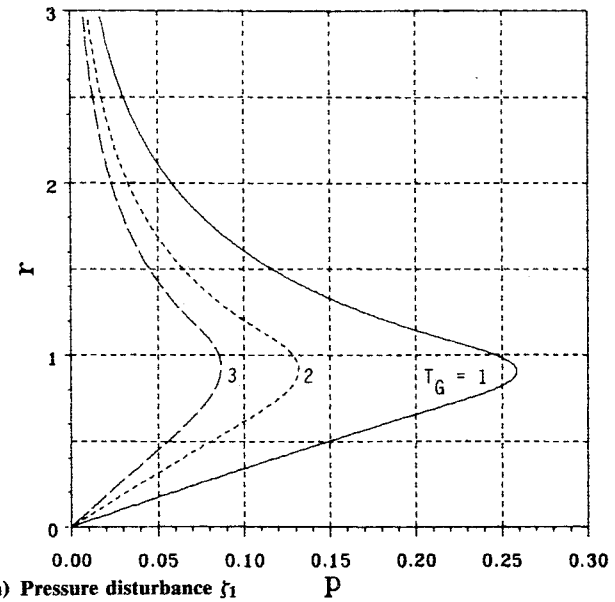

a) Pressure disturbance ζ_1

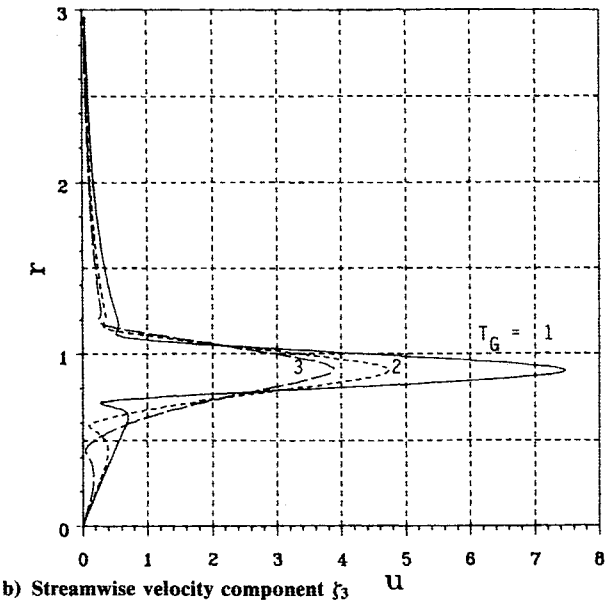

b) Streamwise velocity component ζ_3

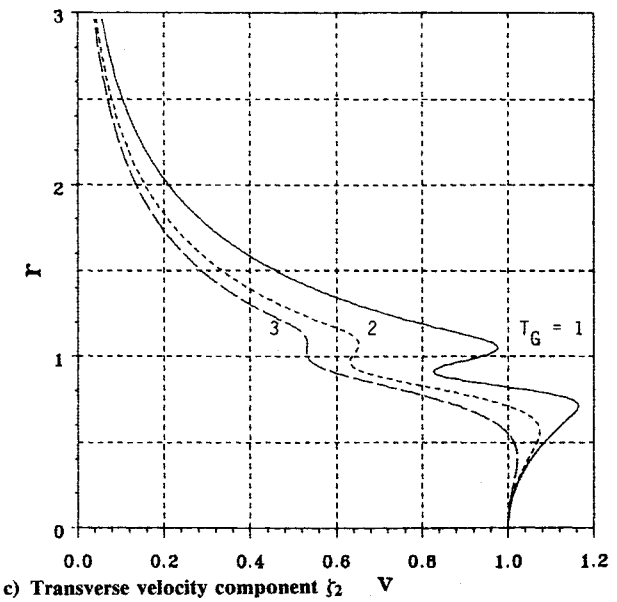

c) Transverse velocity component ζ_2

Fig. 7 First azimuthal mode $m = 1$. Eigenfunctions at $x = 2$, $\omega = 0.8$.

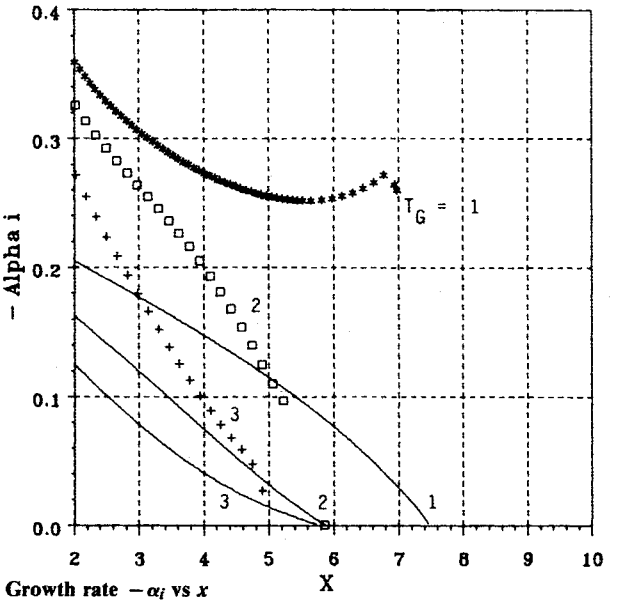

a) Growth rate $-\alpha_i$ vs x

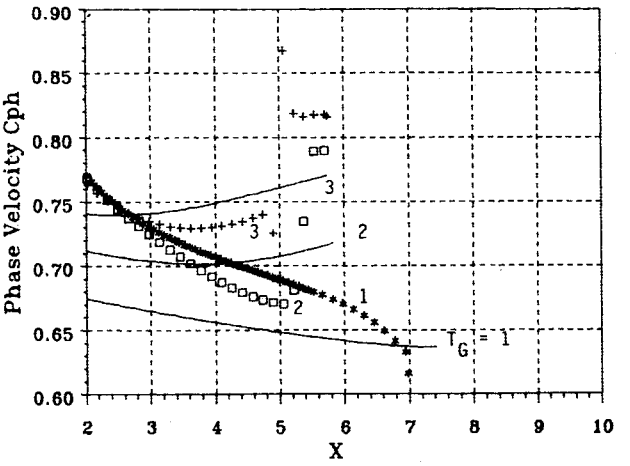

b) Phase velocity c_{ph} vs x; $\omega = 0.8$, $M = 2$

Fig. 8 Axisymmetric mode $m = 0$. Symbols are predictions of nonparallel theory for the pressure at $r = 0.9$.

They determined, in addition to many other results, the x variation of the gain at $r = 0$ for the streamwise velocity component relative to the initial station $x_0 = 2$. The results for $m = 0$ at frequencies $\omega = 0.6$ and 0.9 are compared with the present computation in Fig. 2. The agreement is very good for $\omega = 0.9$, but for $\omega = 0.6$ there is a slight difference for $x > 10$.

Results for Coaxial Mixing Layer

Mean Flow Profiles

The mean flow profiles in the coaxial mixing layer are computed by the method presented in Sec. II. Here, sample results of these profiles are presented. For $M = 2$, $U_G = 0.5$, $T_G = 2$ (or $R_G = 0.5$), the streamwise velocity, density, and transverse velocity profiles at different axial stations are shown in Figs. 3a–3c, respectively. The velocity profiles are nonsimilar, and the potential core extends to $x \approx 6$ (i.e., 3 nozzle diameters). The transverse component that is always negative has a maximum of 2.5% at $x = 1$, and it decays as x increases.

Variation of the Growth Rate with Frequency at the Axial Station $x = 2$

The dependence of the parallel and nonparallel growth rates on the frequency has been computed at the three Mach numbers $M = 1, 2, 3$, the temperature ratios $T_G = 1, 2, 3$, and the

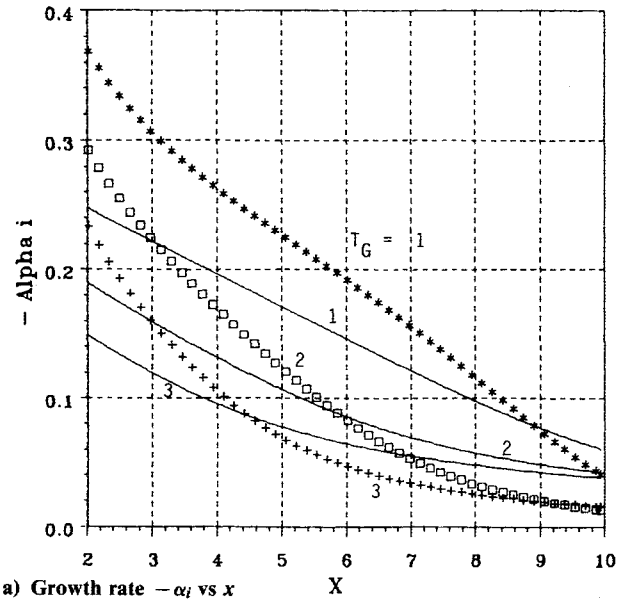

a) Growth rate $-\alpha_i$ vs x

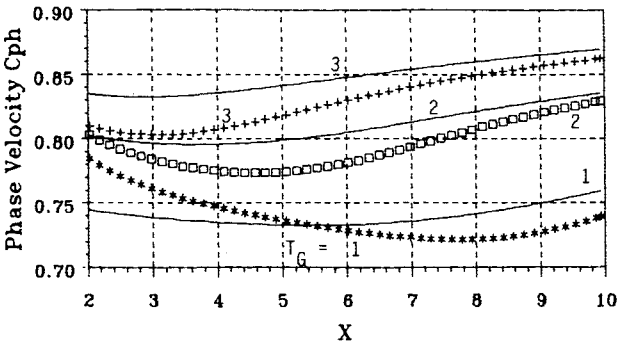

b) Phase velocity c_{ph} vs x; $\omega = 0.8$, $M = 2$

Fig. 9 First azimuthal mode $m = 1$. Symbols are predictions of nonparallel theory for the pressure at $r = 0.9$.

velocity ratio $U_G = 0.5$. Both axisymmetric ($m = 0$) and first azimuthal ($m = 1$) modes are considered. All results are obtained at the axial location $x = 2$. The results are depicted in Figs. 4a–4c for $m = 0$, and in Figs. 5a–5c for $m = 1$. The growth rates of the nonparallel calculations are based on the pressure disturbance at the radial location where the amplitude of p_0 is maximum, which is roughly $r \approx 0.9$ for most cases.

We have to mention here that whenever the parallel calculations indicate near neutral disturbance, that is, when $|-\alpha_i|$ is small, the corresponding nonparallel results show doubtful trend. Such a trend is shown in Figs. 4b and 5b for $T_G = 1$ and $\omega > 3$. Crighton and Gaster[27] and Plaschko[28] also have alluded to numerical difficulties in the nonparallel calculations. It is possible that for near neutral disturbances, the critical point becomes close to the real r axis and, hence, integration along the real axis is affected by the presence of the singularity. However, further investigation of the numerical difficulties is required.

Evident in Figs. 4 and 5 is the significant destabilizing effect produced by the streamwise gradient of the mean flow (i.e., nonparallel effect). That effect is most important for $T_G = 1.0$. However, increasing the Mach number or increasing the temperature of the inner stream (gas generator) reduces the growth rate predicted by both the parallel and the nonparallel calculations.

Eigenfunctions at $x = 2$ for $M = 2$ and $\omega = 0.8$

It is interesting to determine the effect of the temperature profiles on the radial distribution of the disturbances. At

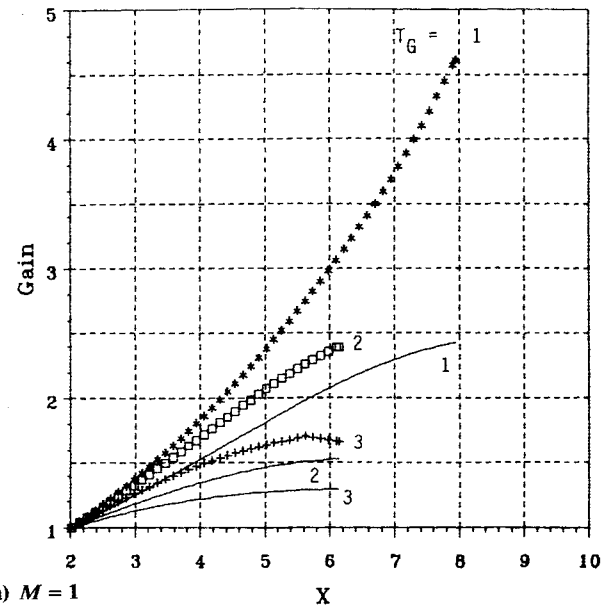

a) $M = 1$

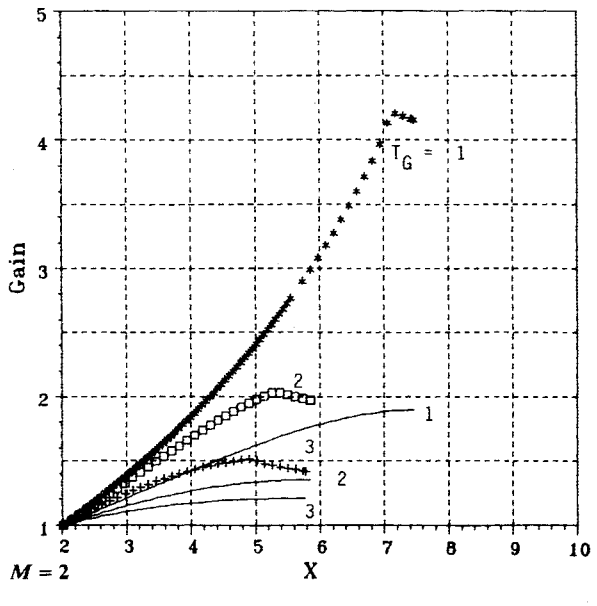

b) $M = 2$

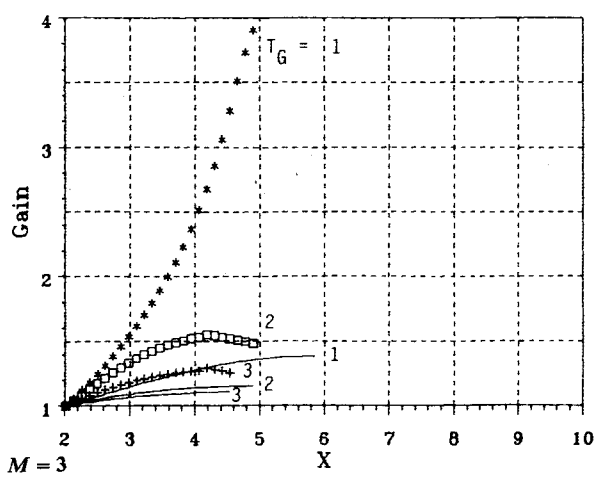

c) $M = 3$

Fig. 10 Axisymmetric mode $m = 0$. Gain in pressure vs x relative to $x = 2$ for $\omega = 0.8$. Symbols are predictions of nonparallel theory for the pressure at $r = 0.9$.

$x = 2$ and for Mach number $M = 2$ and frequency $\omega = 0.8$, the pressure, axial velocity, and radial velocity amplitude distributions are depicted in Figs. 6a–6c for $m = 0$ and Figs. 7a–7c for

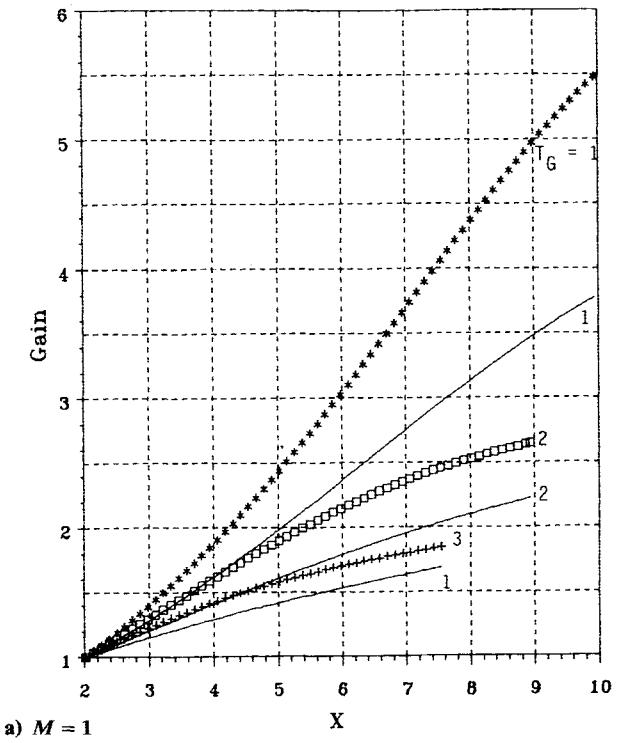

a) $M = 1$

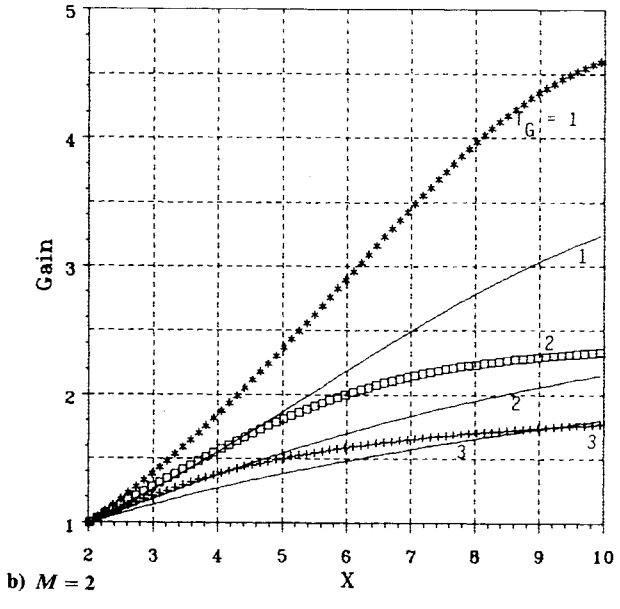

b) $M = 2$

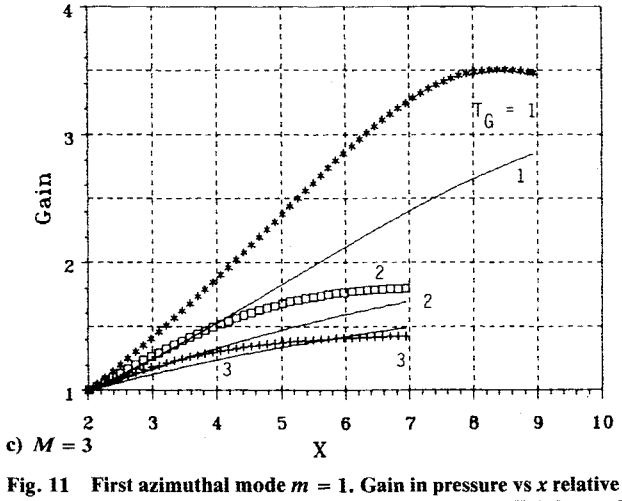

c) $M = 3$

Fig. 11 First azimuthal mode $m = 1$. Gain in pressure vs x relative to $x = 2$ for $\omega = 0.8$. Symbols are predictions of nonparallel theory for the pressure at $r = 0.9$.

$m = 1$. The eigenfunctions are normalized such that $p_0 = 1$ at $r = 0$ when $m = 0$, and $v_0 = 1$ at $r = 0$ when $m = 1$. From Figs. 6a and 7a, we observe that the temperature ratio has little effect on the radial distribution of the pressure disturbance for $m = 0$ but has a significant effect for $m = 1$. For $m = 0$, we observe in Fig. 6b that increasing the inner stream temperature increases the u disturbance near the axis ($r = 0$) and reduces its peak near the mixing zone near $r = 1$. Also for $m = 1$, the maximum of the streamwise velocity disturbance is reduced as the temperature increases. One also should observe the relative magnitudes of the u and v disturbances, for $T_G = 1$, u_{max} is about five times v_{max}.

Variation of the Growth Rate, Phase Speed, and Gain with x at $\omega = 0.8$

For the purpose of the control of spatially developing shear layers, it is required to determine the growth rate and gain along the axis of the layer, and to determine the most amplified frequency. For $M = 2$ and $\omega = 0.8$, the x variation of the growth rate of pressure at $r = 0.9$ is shown in Fig. 8a for $m = 0$ and in Fig. 9a for $m = 1$. The corresponding phase speed distributions are shown in Fig. 8b and Fig. 9b. We observe in Fig. 8a that for the axisymmetric mode $m = 0$, the parallel stability predicts neutral disturbance at $x \approx 5.8$ when $T_G = 2$ and 3, and at $x \approx 7.4$ when $T_G = 1$. These x locations correspond roughly to the end of the potential core. However, for the first azimuthal mode $m = 1$, amplified disturbance is predicted for all x up to $x = 10$. The nonparallel results indicate higher growth rates over most of the x range in Fig. 9a, but for $T_G = 3$ the trend is reversed for $x > 5$ where the growth rate becomes less than that predicted by parallel theory. As shown in Fig. 9b, the phase speed shows weak variation with x for $m = 1$.

Finally, the gain in the pressure relative to the initial x station $x_0 = 2$ and at $r = 0.9$ [see Eq. (40)] is presented. The results for the axisymmetric mode $m = 0$ are shown in Figs. 10a–10c for the Mach numbers $M = 1$, 2, and 3, respectively. Similar results for $m = 1$ are shown in Figs. 11a–11c. Significant contribution from the nonparallelism of the mean flow is evident in these figures. The gain of the first azimuthal mode is larger than that of the axisymmetric mode over the Mach number and temperature ratio ranges considered. Thus, we expect the first azimuthal mode to be the dominant one. However, the gain associated with the compressible mixing layers is much weaker than that of incompressible shear layers. For example, from Fig. 11b the gain according to the nonparallel theory at $x = 10$ relative to $x = 2$ is only a factor of 2.4 when $M = 2$ and $T_G = 2$.

Further work is needed to determine the frequency that maximizes the gain over certain axial length of the shear layer.

Conclusions

The characteristics of instability waves on the shear layer of a coaxial mixing configuration at supersonic speed are determined. We conclude the following:

1) The nonparallelism of the basic state has significant effect on the growth rate of both axisymmetric and first azimuthal modes.

2) The axisymmetric mode ($m = 0$) is damped for axial stations downstream of the core region, and the first azimuthal mode dominates.

3) Increasing the outer stream Mach number or increasing the inner stream temperature reduces the growth rate of both modes.

The above conclusions are consistent with previously published results for the supersonic jet problem (e.g., Ref. 19).

Acknowledgment

This work was supported by the Office of Naval Research under Contract N00014-87-K-0168.

References

[1]Ferri, A., "Supersonic Combustion Progress," *Aeronautics and Astronautics,* Vol. 2, Aug. 1964, pp. 32-37.

[2]Billing, F. S., "Ramjets with Supersonic Combustion," *AGARD Lecture Series 136,* 1984, pp. 8-1-8-29.

[3]Waltrup, P. J., "Liquid Fueled Supersonic Combustion Ramjets: A Research Perspective of the Past, Present and Future," AIAA Paper 86-0158, Jan. 1986.

[4]Billing, F. S., Waltrup, P. J., and Stockbridge, R. D., "The Integral Rocket Dual Combustion Ramjet: A New Propulsion Concept," *Journal of Spacecraft and Rockets,* Vol. 17, May 1980, pp. 416-424.

[5]Ikawa, H. and Kubota, T., "Investigation of Supersonic Turbulent Mixing Layer with Zero Pressure Gradient," *AIAA Journal,* Vol. 13, May 1975, pp. 566-572.

[6]Chinzei, N., Masuya, G., Komuro, T., Murakami, A., and Kudou, K., "Spreading of Two-Stream Supersonic Turbulent Mixing Layers," *The Physics of Fluids,* Vol. 29, May 1986, pp. 1345-1347.

[7]Ho, E. M. and Huerre, P., "Perturbed Free Shear Layers," *Annual Review of Fluid Mechanics,* Vol. 16, 1984, pp. 365-424.

[8]Breidenthal, R., "Structure in Turbulent Mixing Layers and Wakes Using a Chemical Reaction," *Journal of Fluid Mechanics,* Vol. 109, Aug. 1981, pp. 1-24.

[9]Jimenez, J., "A Spanwise Structure in the Plane Shear Layer," *Journal of Fluid Mechanics,* Vol. 132, July 1983, pp. 319-336.

[10]Brown, G. L. and Roshko, A., "On Density Effects and Large Structure in Turbulent Mixing Layers," *Journal of Fluid Mechanics,* Vol. 64, July 1974, pp. 775-816.

[11]Papamoschou, D. and Roshko, A., "Observations of Supersonic Free Shear Layers," AIAA Paper 86-0162, Jan. 1986.

[12]Ho, C. H. and Huang, L. S., "Subharmonic and Vortex Merging in Mixing Layers," *Journal of Fluid Mechanics,* Vol. 119, June 1982, pp. 443-473.

[13]Gaster, M., Kit, E., and Wygnanski, I., "Large Scale Structures in a Forced Turbulent Mixing Layer," *Journal of Fluid Mechanics,* Vol. 150, Jan. 1985, pp. 23-29.

[14]Wygnanski, I. and Petersen, R. A., "Coherent Motion in Excited Free Shear Flows," AIAA Paper 85-0539, 1985.

[15]Wygnanski, I., Champagne, F. H., and Marasli, B., "On the Large Scale Structures in Two-Dimensional Small Deficit, Turbulent Wakes," *Journal of Fluid Mechanics,* Vol. 168, July 1986, pp. 31-71.

[16]Cohen, J., "Instabilities and Resonances in Turbulent Free Shear Flows," Ph.D. Thesis, Univ. of Arizona, Tucson, AZ, 1986.

[17]Tam, C. K. W. and Morris, P. J., "The Radiation of Sound by the Instability Waves of a Compressible Plane Turbulent Shear Layer," *Journal of Fluid Mechanics,* Vol. 98, May 1980, pp. 349-381.

[18]Tam, C. K. W. and Burton, D. E., "Sound Generated by Instability Waves of Supersonic Flows: Part 1," *Journal of Fluid Mechanics,* Vol. 138, Jan. 1984, pp. 249-271.

[19]Michalke, A., "Survey on Jet Instability Theory," *Progress in Aerospace Sciences,* Vol. 21, No. 3, Pergamon, London, 1984, pp. 159-199.

[20]Anderson, D. A., Tannehill, J. C., and Pletcher, R. H., *Computational Fluid Mechanics and Heat Transfer,* McGraw-Hill, New York, 1984.

[21]Dash, S. M., Wilmoth, R. G., and Pergament, H. S., "Overlaid Viscous/Inviscid Model for the Prediction of Near-Field Jet Entrainment," *AIAA Journal,* Vol. 17, Sept. 1979, pp. 950-958.

[22]Hasen, G. A., "Navier-Stokes Solutions for an Axisymmetric Nozzle," *AIAA Journal,* Vol. 20, Sept. 1982, pp. 1219-1227.

[23]Nayfeh, A. H., *Perturbation Methods,* Wiley-Interscience, New York, 1973, Chap. 6.

[24]Nayfeh, A. H., *Introduction to Perturbation Techniques,* Wiley-Interscience, New York, 1981.

[25]Saric, W. S. and Nayfeh, A. H., "Nonparallel Stability of Boundary-Layer Flows," *The Physics of Fluids,* Vol. 18, No. 8, 1975, pp. 945-950.

[26]Nayfeh, A. H., "Stability of Three-Dimensional Boundary Layers," *AIAA Journal,* Vol. 18, April 1980, pp. 406-416.

[27]Crighton, D. G. and Gaster, M., "Stability of Slowly Diverging Jet Flow," *Journal of Fluid Mechanics,* Vol. 77, Sept. 1976, pp. 397-413.

[28]Plaschko, P., "Helical Instabilities of Slowly Divergent Jets," *Journal of Fluid Mechanics,* Vol. 92, May 1979, pp. 209-215.

[29]Crow, S. C. and Champagne, F. H., "Orderly Structure in Jet Turbulence," *Journal of Fluid Mechanics,* Vol. 48, 1971, pp. 547-591.